The macrophage odorant receptor Olfr78 mediates the lactate-induced M2 phenotype of tumor-associated macrophages

Sri Murugan Poongkavithai Vadevoo[a,b,c], Gowri Rangaswamy Gunassekaran[a,b,c], ChaeEun Lee[d,e], NaHye Lee[d,e], Jiyoun Lee[f], Sehyun Chae[g], Jae-Yong Park[f], JaeHyung Koo[d,e,1], and Byungheon Lee[a,b,c,1]

[a]Department of Biochemistry and Cell Biology, School of Medicine, Kyungpook National University (KNU), Daegu 41944, Republic of Korea; [b]BK21 FOUR KNU Convergence Education Program, Department of Biomedical Science, School of Medicine, KNU, Daegu 41944, Republic of Korea; [c]CMRI, School of Medicine, KNU, Daegu 41944, Republic of Korea; [d]Department of New Biology, Daegu Gyeongbuk Institute of Science and Technology (DGIST), Daegu 42988, Republic of Korea; [e]New Biology Research Center, DGIST, Daegu 42988, Republic of Korea; [f]BK21 FOUR R&E Center for Learning Health Systems, School of Biosystem and Biomedical Sciences, College of Health Sciences, Korea University, Seoul 02841, Republic of Korea; and [g]Neurovascular Unit Research Group, Korea Brain Research Institute, Daegu 41062, Republic of Korea

Expression and function of odorant receptors (ORs), which account for more than 50% of G protein–coupled receptors, are being increasingly reported in nonolfactory sites. However, ORs that can be targeted by drugs to treat diseases remain poorly identified. Tumor-derived lactate plays a crucial role in multiple signaling pathways leading to generation of tumor-associated macrophages (TAMs). In this study, we hypothesized that the macrophage OR Olfr78 functions as a lactate sensor and shapes the macrophage–tumor axis. Using Olfr78$^{+/+}$ and Olfr78$^{-/-}$ bone marrow–derived macrophages with or without exogenous Olfr78 expression, we demonstrated that Olfr78 sensed tumor-derived lactate, which was the main factor in tumor-conditioned media responsible for generation of protumoral M2-TAMs. Olfr78 functioned together with Gpr132 to mediate lactate-induced generation of protumoral M2-TAMs. In addition, syngeneic Olfr78-deficient mice exhibited reduced tumor progression and metastasis together with an increased anti- versus protumoral immune cell population. We propose that the Olfr78–lactate interaction is a therapeutic target to reduce and prevent tumor progression and metastasis.

GPCR | Olfr78 | TAMs | OR51E2 | lactate

Odorant receptors (ORs) are the largest subfamily of G protein–coupled receptors (GPCRs), accounting for ~400 of more than 800 human GPCRs and 1,000 of an estimated 1,700 mouse GPCRs (1, 2). GPCRs are a major type of drug target and have been extensively studied (3). However, studies have focused on the functions of ORs in the nose, and investigations of their ectopic expression and functions in nonolfactory tissues are lacking (4, 5). The development of next-generation sequencing techniques, such as bulk (6) and single-cell (7, 8) RNA sequencing, has made it possible to detect and analyze genes that are lowly expressed or expressed in certain cell types (4, 5). Consequently, research into the functions of ectopic ORs is growing rapidly, and such ORs have been suggested as potential drug targets (9–11). Nevertheless, studies of ectopic ORs as drug targets in tumors are limited due to the lack of identification and characterization of ORs in pathophysiological conditions in vivo, such as in the tumor microenvironment (TME).

GPCRs are traditionally thought to be monomers, but recent evidence demonstrates they form dimers or oligomers for their normal trafficking and function (12). Few GPCRs strictly require heterodimerization for surface expression and functional activity. Therefore, a detailed study of GPCR heterodimerization as part of their functional activation is of tremendous clinical importance because GPCRs are the molecular targets of numerous therapeutic drugs (12). For instance, heteromerization of Gpr132 (also known as G2A) with other GPCRs enhances ligand sensitivity (13). Gpr132 differentially couples with multiple G proteins, including

Gs, depending on which ligand binds, and this correlates with its ability to induce cyclic adenosine monophosphate elevation (14). An OR was also reported to increase its surface expression through heterodimerization with its partner GPCR (15). However, it is unknown whether an ectopic OR functions by heteromerizing with GPCRs in pathophysiological conditions.

Tumor-associated macrophages (TAMs) are one of the main components of the TME and promote tumor progression, angiogenesis, invasion, metastasis, and immunosuppression (16–18). Macrophages differentiate into protumoral M2-TAMs in response to stimuli such as lactate (19), interleukin (IL)-4, IL-13, IL-10, macrophage colony-stimulating factor, and corticosteroids (20) in the TME. Lactate produced in the tumor landscape is transported by monocarboxylate transporters expressed in various cell types and used as a carbon source by lactate dehydrogenase (21). It also acts as a signaling molecule that binds to GPCRs (22). Lactate affects many cell types, including macrophages, effector T cells, and regulatory T cells (Tregs), in the TME (21). Among these, macrophage polarization to generate protumoral M2-TAMs plays a crucial role in immunomodulation in the TME, which in turn promotes tumor progression and metastasis (19). However, cross-talk between lactate and macrophages leading to generation of

Significance

Expression and function of odorant receptors (ORs) are being increasingly reported in nonolfactory sites. However, ORs that can be targeted by drugs to treat diseases remain poorly identified. Here, we hypothesized that the macrophage OR Olfr78 functions as a tumor-derived lactate sensor and shapes the macrophage–tumor axis. Olfr78 and the G protein–coupled receptor Gpr132 form a heterodimer that senses lactate in the tumor microenvironment, leading to generation of tumor-associated macrophages with a protumoral M2 phenotype, which promotes tumor progression and metastasis. Our findings suggest an alternative strategy for cancer treatment, namely targeting the interaction between tumor-derived metabolites and ORs.

protumoral M2-TAMs that enhance tumor progression remains poorly defined.

In this study, we hypothesized that the lactate-activated OR Olfr78 (OR51E2, a human analog) functions as a macrophage lactate sensor. We sought to determine whether Olfr78 on bone marrow–derived macrophages (BMDMs) senses tumor-derived lactate and mediates lactate-induced M2 polarization. To strengthen our study of the role of Olfr78 as a lactate sensor on macrophages, we used *Olfr78*^{−/−} mice. We also sought to identify factors in tumor-conditioned media (TCM) that are sensed by Olfr78 and found that lactate and, under some conditions, acetate in TCM were the main factors involved in Olfr78-mediated generation of protumoral M2-TAMs. Furthermore, we showed that Olfr78 formed a heterodimer with Gpr132 to enhance its surface expression and mediated the lactate-induced M2 phenotype of TAMs. Finally, we demonstrated that Olfr78 deficiency inhibited tumor progression and metastasis and favored antitumor immunity in vivo. Based on our results, we propose that the Olfr78–lactate interaction plays a key role in tumor progression and thus targeting the Olfr78–lactate axis is a promising approach for targeted cancer therapy.

Results

Olfr78 Senses Lactate and Mediates Lactate-Induced M2 Polarization of Macrophages.
Lactate activates Olfr78 in a dose-dependent manner and has a half-maximal effective concentration (EC_{50}) of 4 to 21 mM (23, 24). To examine the involvement of Olfr78 in lactate-induced M2 polarization of macrophages, we investigated whether it was expressed in BMDMs isolated from *Olfr78*^{+/+} (wild-type; WT) and *Olfr78*^{−/−} mice. Approximately 43 and 1% of BMDMs isolated from WT and *Olfr78*^{−/−} mice expressed Olfr78, respectively (Fig. 1*A*). The concentration of lactate in TCM of human and mouse tumor cells was ∼8 to 20 mM (*SI Appendix*, Fig. S1*A*). Therefore, the concentration of lactate produced in tumors is similar to the physiological concentration range of lactate that activates Olfr78 (23, 24). Next, we differentiated BMDMs into M1 and M2 macrophages to investigate whether the expression level of Olfr78 was regulated according to macrophage polarization. Lactate, TCM, and IL-4 (19, 25) were used to stimulate M2 polarization, while lipopolysaccharide (LPS) plus interferon (IFN)-γ (L+I) (26) was used to stimulate M1 polarization. Olfr78 expression significantly (*P* < 0.01) increased upon differentiation of BMDMs into M2 macrophages in response to lactate, TCM, and IL-4 but significantly (*P* < 0.05) decreased upon L+I–induced M1 polarization (Fig. 1*B* and *SI Appendix*, Fig. S1*B*), suggesting that Olfr78 is an M2 macrophage marker. To investigate the effect of Olfr78 on macrophage polarization, we measured the protein levels of M2 macrophage markers such as CD206 (Fig. 1*C* and *SI Appendix*, Fig. S1*B*) and the messenger RNA (mRNA) levels of *IL-4*, *IL-10*, and *transforming growth factor* β (*TGF*-β) (Fig. 1 *E*–*G*), as well as M1 macrophage markers such as CD86 (Fig. 1*D* and *SI Appendix*, Fig. S1*B*) and the mRNA levels of *IL-12* and *IFN*-γ (Fig. 1 *H* and *I*) when WT and *Olfr78*^{−/−} BMDMs were differentiated into M1 and M2 macrophages. The protein level of CD206 (Fig. 1*C*) and the mRNA levels of *IL-4*, *IL-10*, and *TGF*-β (Fig. 1 *E*–*G*) were dramatically (*P* < 0.001) higher and the protein level of CD86 (Fig. 1*D* and *SI Appendix*, Fig. S1*B*) and the mRNA levels of *IL-12* and *IFN*-γ (Fig. 1 *H* and *I*) were significantly (*P* < 0.001) lower in lactate-treated WT BMDMs than in untreated BMDMs (-). Similarly, TCM and IL-4 treatment up-regulated (*P* < 0.001) CD206 and down-regulated CD86 in WT BMDMs, while L+I treatment elicited the opposite effects (Fig. 1 *C* and *D*). However, lactate-treated *Olfr78*^{−/−} BMDMs did not exhibit up-regulation of M2-specific markers or down-regulation of M1-specific markers compared with untreated BMDMs (Fig. 1 *C*–*I*). IL-4 treatment still up-regulated CD206 (Fig. 1*C*) and down-regulated CD86 (Fig. 1*D*) in *Olfr78*^{−/−} BMDMs, suggesting that Olfr78 is required for lactate- and TCM-induced, but not IL-4–induced, M2 polarization of macrophages. Next, we restored

Olfr78 expression in *Olfr78*^{−/−} BMDMs by transfecting them with a Flag-tagged Olfr78 expression vector. Immunostaining using anti-Flag and anti-Olfr78 antibodies demonstrated expression of exogenous Olfr78 in transfected *Olfr78*^{−/−} BMDMs (Fig. 1*J*). Exogenous Olfr78 expression in *Olfr78*^{−/−} BMDMs partly (*P* < 0.01) restored the lactate-induced changes in mRNA levels of cytokines compared with WT and *Olfr78*^{−/−} BMDMs (Fig. 1 *E*–*I*).

To examine the effect of ORs on M2 polarization of human macrophages, THP-1 human immortalized monocytes were treated with phorbol myristate acetate (PMA) and then with L+I, IL-4, TCM, or lactate. The protein (*SI Appendix*, Fig. S2*A*) and mRNA (*SI Appendix*, Fig. S2*B*) levels of OR51E2, a human analog of mouse Olfr78, in THP-1 cells significantly (*P* < 0.01) increased upon treatment with lactate, TCM, and IL-4 but decreased (*P* < 0.05) upon treatment with L+I, suggesting that OR51E2 was induced in M2-polarized human macrophages, similar to mouse Olfr78. Similar to IL-4 and TCM, lactate treatment increased the levels of M2 macrophage markers such as Arg1, CD206, CD163, and *IL-10* in THP-1 cells (*SI Appendix*, Figs. S2 *C*–*G* and S14*A*). On the other hand, it did not affect the levels of M1 macrophage markers such as CD86, *TNF*-α, and *IL-12B* (*SI Appendix*, Fig. S2 *H*–*J*), and decreased the level of inducible nitric oxide synthase (iNOS) compared with untreated cells (*SI Appendix*, Figs. S2 *C* and *D* and S14*A*).

Next, we depleted *OR51E2* in THP-1 cells. Transfection of an *OR51E2*-targeting small interfering RNA (siRNA) decreased the OR51E2 protein level (*SI Appendix*, Figs. S3 *A* and *B* and S14*B*) and the percentage of OR51E2-expressing cells (*SI Appendix*, Fig. S3*C*). Compared with untreated cells, lactate treatment did not up-regulate M2 markers such as Arg-1, CD163, CD206, and *IL-10* (*SI Appendix*, Figs. S3 *D*–*H* and S14*C*) or down-regulate M1 markers such as iNOS (*SI Appendix*, Figs. S3 *D* and *E* and S14*C*), CD86, *TNF*-α, and *IL-12*B (*SI Appendix*, Fig. S3 *I*–*K*) in *OR51E2*-depleted THP-1 cells. IL-4 treatment still up-regulated M2 markers (*SI Appendix*, Fig. S3 *D*–*H*) and L+I treatment up-regulated M1 markers such as CD86, *TNF*-α, and *IL-12B* (*SI Appendix*, Fig. S3 *I*–*K*) in *OR51E2*-depleted THP-1 cells. Taken together, these results suggest that OR51E2 is required for lactate- and TCM-induced, but not IL-4–induced, M2 polarization of human macrophages.

Lactate and Acetate Are the Main Factors in TCM Responsible for Olfr78-Mediated M2 Macrophage Polarization.
Lactate is critical for M2 macrophage polarization (19, 21). To determine whether it is the main factor in TCM responsible for Olfr78-mediated M2 macrophage polarization, we treated WT BMDMs with TCM of mouse tumor cell lines pretreated with oxamic acid (OA), an inhibitor of lactate dehydrogenase that prevents lactate production (27). Pretreatment with OA almost completely (*P* < 0.001) depleted lactate in TCM (Fig. 2*A*). Compared with untreated BMDMs, lactate- and TCM-treated WT BMDMs exhibited significant up-regulation (*P* < 0.001) of M2 polarization markers, such as CD206, IL-4, IL-10, and TGF-β (Fig. 2 *B*–*E*), and an increase (*P* < 0.001) in the percentage of cells with an elongated shape (Fig. 2 *F* and *G*). Up-regulation of M2 markers was attenuated (*P* < 0.05) in WT BMDMs treated with lactate-depleted TCM (TCM+OA). Such changes in the levels of M2 markers were not observed in *Olfr78*^{−/−} BMDMs (Fig. 2 *B*–*G*). Addition of exogenous lactate to lactate-depleted TCM (TCM+OA+LA) restored (*P* < 0.05) M2 polarization of WT, but not of *Olfr78*^{−/−}, BMDMs (Fig. 2 *B*–*G*). We suggest that lactate is the main factor in TCM responsible for Olfr78-mediated M2 macrophage polarization. To investigate whether the increase in cytokines is due to an increase in cell number after treatment with TCM or exogenous lactate, the percentage viability of BMDMs was analyzed by the trypan blue assay (*SI Appendix*, Fig. S4). BMDMs, which are primary monocyte–derived macrophage cells, proliferated less after
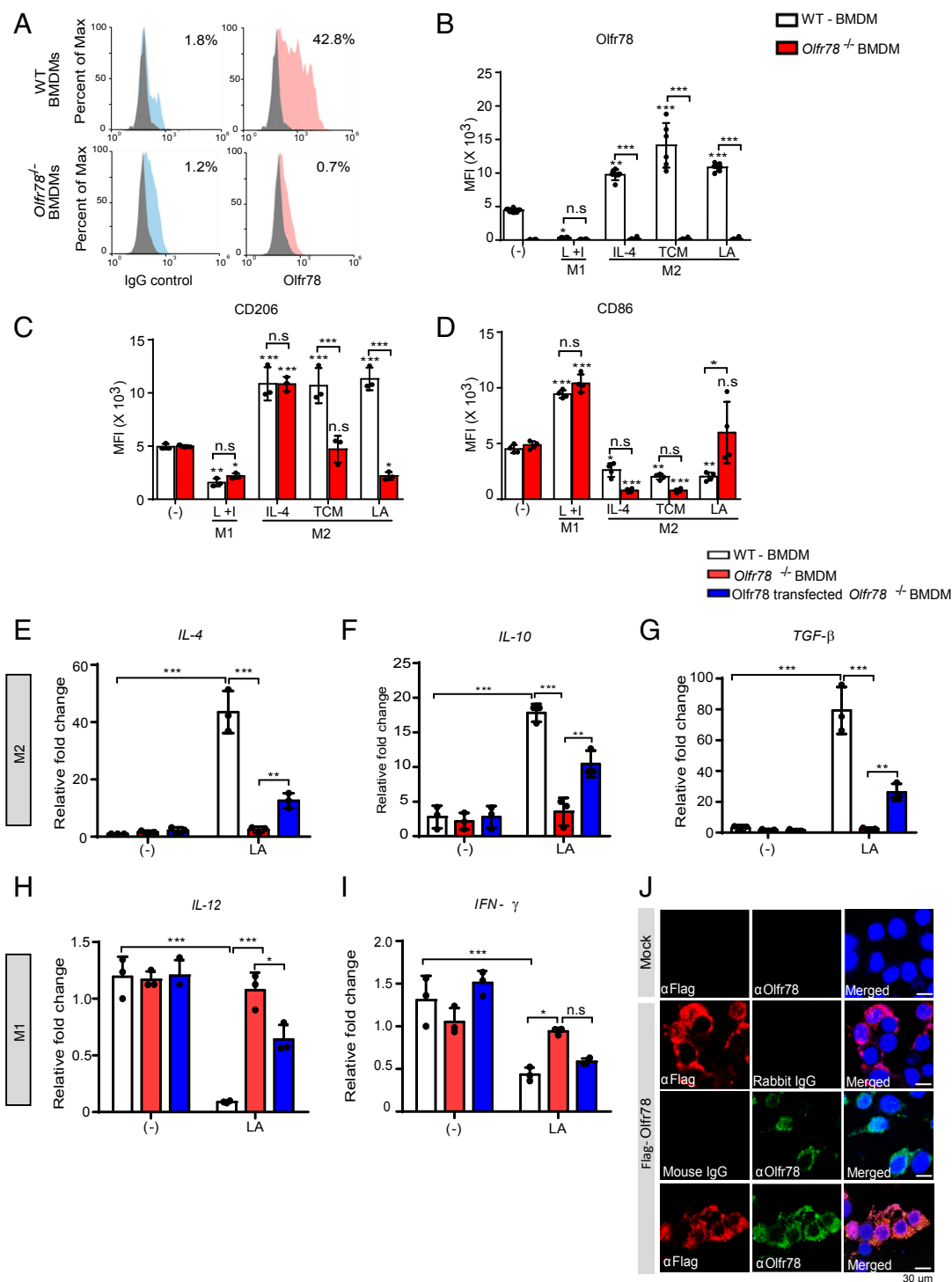
Fig. 1. Olfr78 mediates lactate-induced M2 polarization of mouse BMDMs. (*A*) Flow cytometric analysis of Olfr78 expression in BMDMs isolated from WT and *Olfr78*$^{-/-}$ mice. Surface expression of Olfr78 (pink histograms) is presented in comparison with unstained cells (gray histograms). Rabbit IgG (blue histograms) was used as a control. Data are representative of three independent experiments. (*B–D*) Flow cytometric analysis of Olfr78 (*B*), the M2 marker CD206 (*C*), and the M1 marker CD86 (*D*) in BMDMs isolated from WT and *Olfr78*$^{-/-}$ mice at 48 h after treatment with LPS (100 ng/mL) plus recombinant mouse IFN-γ (20 ng/mL) to induce M1 polarization and with recombinant mouse IL-4 (20 ng/mL), tumor-conditioned media, or lactate (10 mM) to induce M2 polarization. Untreated BMDMs were used as a control (-). Data represent mean ± SD of $n = 3$ to 6 wells per condition from a representative of three independent experiments. (*E–I*) qRT-PCR analysis of the mRNA levels of *IL-4* (*E*), *IL-10* (*F*), and *TGF*-β (*G*) for M2 polarization and *IL-12* (*H*) and *IFN*-γ (*I*) for M1 polarization in WT, *Olfr78*$^{-/-}$, and exogenous Olfr78-expressing *Olfr78*$^{-/-}$ BMDMs treated with or without lactate for 48 h. Data represent mean ± SD of triplicate wells from a representative of four independent experiments. (*J*) Immunofluorescence microscopic analysis of *Olfr78*$^{-/-}$ BMDMs transfected with a Flag-tagged Olfr78 expression vector. Flag (red) and Olfr78 (green) staining is shown together with DAPI counterstaining. Images are representative of three independent experiments. (Scale bars, 30 µm.) MFI, mean fluorescence intensity; n.s, not significant. *$P < 0.05$, **$P < 0.01$, and ***$P < 0.001$ compared with the untreated control in each condition unless denoted. Statistical analyses were performed using a two-way ANOVA with the Bonferroni multiple-comparison test.
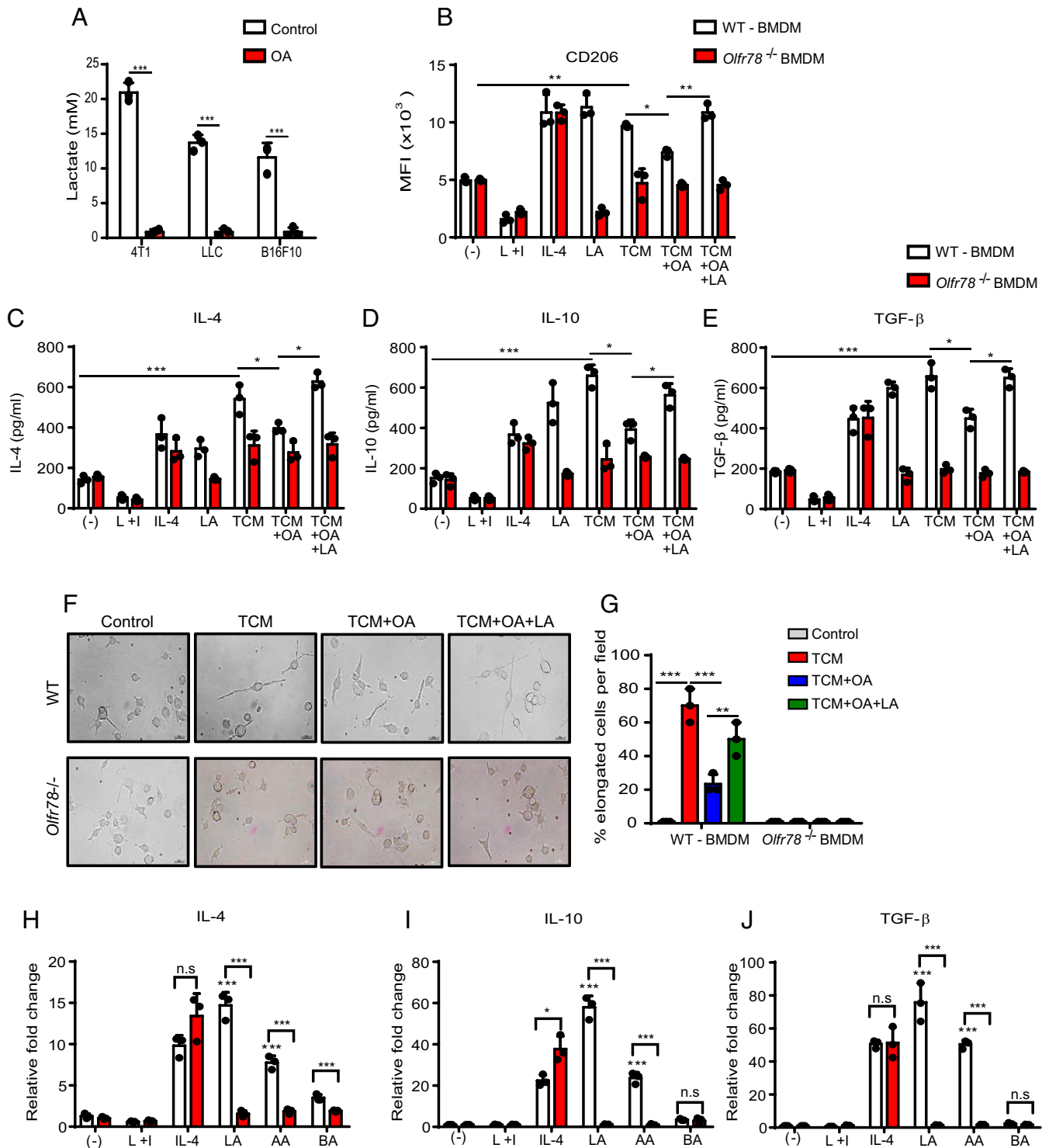
Fig. 2. Lactate and acetate, but not butyrate, are key molecules in TCM-induced M2 polarization of mouse BMDMs. (*A*) Lactate concentrations in TCM collected after culture of mouse tumor cells (4T1, LLC, and B16F10) in the presence of OA (90 mM) for 72 h and an additional 24 h without OA. Data represent mean ± SD of triplicate wells from a representative of three independent experiments. (*B*) Flow cytometric analysis of the M2 marker CD206 in BMDMs isolated from WT (white bars) and *Olfr78*^{−/−} (red bars) mice at 48 h after treatment with L+I, IL-4, LA, TCM, OA-treated TCM (TCM+OA), and OA-treated TCM with exogenous addition of lactate (10 mM) (TCM+OA+LA). Untreated BMDMs were used as a control (-). (*C*–*E*) ELISAs to measure the concentrations of the M2-specific cytokines IL-4 (*C*), IL-10 (*D*), and TGF-β (*E*) in cultures of BMDMs isolated from WT (white bars) and *Olfr78*^{−/−} (red bars) mice after the various treatments. (*F*) Morphology (elongated shape) of BMDMs isolated from WT and *Olfr78*^{−/−} mice after the various treatments for 48 h. Images are representative of three independent experiments. (Scale bars, 20 μm.) (*G*) The percentage of elongated cells per field. This was calculated using the following formula: % elongated cells = (number of elongated cells per field/total number of cells per field) × 100. (*H*–*J*) qRT-PCR analysis of the mRNA levels of the M2-specific markers *IL-4* (*H*), *IL-10* (*I*), and *TGF*-β (*J*) in BMDMs isolated from WT (white bars) and *Olfr78*^{−/−} (red bars) mice after treatment with lactate (10 mM), acetate (AA; 10 mM), or butyrate (BA; 10 mM). Data represent mean ± SD of triplicate wells from a representative of three independent experiments. *$P <$ 0.05, **$P <$ 0.01, and ***$P <$ 0.001 compared with the untreated control (-) in each condition unless denoted. Statistical analyses were performed using a two-way ANOVA with the Bonferroni multiple-comparison test.

treatment. Similar changes in the levels of M2 markers, such as Arg1, CD206, CD163, *IL-10*, and *CD206*, upon treatment with lactate-depleted TCM of human tumor cells (TCM+OA) and following addition of exogenous lactate to TCM (TCM+OA+LA) were observed in parental and *OR51E2*-depleted THP-1 immortalized human monocytes (*SI Appendix*, Figs. S5 and S14*D*).

In addition, we examined the effect of acetate, the other short-chain fatty acid that acts as a ligand of Olfr78 (23, 24, 28), on M2 polarization of macrophages. Similar to lactate, acetate treatment significantly ($P < 0.001$) increased the mRNA levels of M2 markers such as *IL-4*, *IL-10*, and *TGF*-β in WT BMDMs, but treatment with butyrate, which does not interact with Olfr78 (28), did not (Fig. 2 *H–J*). Acetate did not induce M2 polarization of *Olfr78*$^{-/-}$ BMDMs (Fig. 2 *H–J*), suggesting that Olfr78 mediates both lactate- and acetate-induced M2 polarization of macrophages.

Olfr78 Cooperates with Gpr132 to Mediate Lactate-Induced M2 Polarization of Macrophages. Gpr132 was reported to detect lactate and mediate M2 polarization of macrophages (22). We hypothesized that Olfr78 and Gpr132 function together to mediate lactate-induced M2 polarization of macrophages. To investigate this, we examined the colocalization of Olfr78 and Gpr132 in M1 and M2 macrophages and BMDMs. Gpr132 was expressed in M1 and M2 macrophages and BMDMs (Fig. 3*A*). By contrast, Olfr78 was expressed in BMDMs and M2 macrophages, where it colocalized with Gpr132, but not in M1 macrophages (Fig. 3*A*). To investigate the physical proximity of Olfr78 and Gpr132, a proximity ligation assay (PLA) using anti-Olfr78 and anti-Gpr132 antibodies was performed. This demonstrated a direct interaction between Olfr78 and Gpr132 on the membrane of BMDMs and M2 macrophages, but not of M1 macrophages (Fig. 3*B*). In addition, Olfr78 was coimmunoprecipitated by an anti-Gpr132 antibody and Gpr132 was coimmunoprecipitated by an anti-Olfr78 antibody (Fig. 3*C* and *SI Appendix*, Fig. S14*E*). Consistently, the high bioluminescence resonance energy transfer (BRET) ratios of Olfr78:GPR132 were significantly ($P < 0.001$) similar to those of TREK1:TWIK1 (Fig. 3*D* and *SI Appendix*, Fig. S6), which is a positive control (29, 30). The interaction of Olfr78 with the β$_2$-adrenergic receptor (ADRB2), a potential negative control that has not been reported to interact with Olfr78 in the TAM, was negligible (Fig. 3*D* and *SI Appendix*, Fig. S6). Relative luciferase activity upon treatment with sodium lactate was higher in Hana3A cells cotransfected with Olfr78 and Gpr132 (Fig. 3*E*, red) than in those transfected with Olfr78 or Gpr132 alone. Sodium acetate showed the most luciferase activity in Olfr78 and Gpr132 cotransfection as a positive ligand control (Fig. 3*E*). Taken together, these results suggest that Olfr78 and Gpr132 form a functional heterodimer. To further analyze whether Gpr132 acts as a chaperone for Olfr78 expression, Rho-tagged Olfr78 was cotransfected with Gpr132 or a mock vector. Expression of Rho-Olfr78 was significantly ($P < 0.01$) higher in cells cotransfected with Gpr132 than in cells cotransfected with the mock vector (Fig. 3 *F* and *G*). In addition, analysis of cells transfected with OR51E2 with or without Gpr132 and activated using lactate revealed that OR51E2 alone could not be activated by lactate, and lactate-mediated activation was highly dependent on dual expression of OR51E2 and Gpr132 (*SI Appendix*, Fig. S7). These results indirectly demonstrate that both receptors are required for lactate-mediated activation.

To investigate whether Olfr78 and Gpr132 cooperate to mediate lactate-induced M2 polarization, we depleted *Gpr132* in WT and *Olfr78*$^{-/-}$ BMDMs (*SI Appendix*, Figs. S8 and S14*F*). Lactate-induced up-regulation of the mRNA levels of M2 cytokines such as *IL-4*, *IL-10*, *TGF*-β, and *Arg1* was significantly ($P < 0.01$) reduced in *Gpr132*-depleted WT BMDMs (Fig. 3 *H–K*). The mRNA levels of *IL-4*, *IL-10*, and *TGF*-β were further reduced in *Gpr132*-depleted *Olfr78*$^{-/-}$ BMDMs (Fig. 3 *H–J*). These

results suggest that Olfr78 and Gpr132 cooperate to mediate lactate-induced M2 polarization of macrophages.

Deficiency of Olfr78 Inhibits Tumor Progression and Favors Antitumor Immunity In Vivo. To examine the involvement of Olfr78 in tumor progression in vivo, we established syngeneic lung tumors in WT and *Olfr78*$^{-/-}$ mice. Upon subcutaneous implantation of Lewis lung carcinoma (LLC) cells, tumor growth was significantly ($P < 0.001$) slower (Fig. 4*A*), the survival rate was significantly ($P < 0.001$) better (Fig. 4*B*), and the number of metastatic nodules in the lung was significantly ($P < 0.001$) lower (Fig. 4*C*) in *Olfr78*$^{-/-}$ mice than in WT mice. The tumor immune cell population was gated using the leukocyte marker CD45 and analyzed further (*SI Appendix*, Fig. S9). The populations of total macrophages (Fig. 4*D*) and immunosuppressive cells including CD45+Ly6C−MHCII− M2-polarized TAMs (Fig. 4*E*), CD45+Gr1+CD11b+ myeloid-derived suppressor cells (MDSCs) (Fig. 4*G*), and CD3+CD4+Foxp3+ Tregs (Fig. 4*H*) were significantly ($P < 0.001$) smaller in tumor tissues of *Olfr78*$^{-/-}$ mice than in tumor tissues of WT mice. On the other hand, the populations of immunostimulatory cells including CD45+Ly6C−MHCII+ M1-polarized macrophages (Fig. 4*F*), CD3+CD4−CD8+ T cells (Fig. 4*I*), and CD3+CD4+CD8− T cells (Fig. 4*J*) were larger in tumor tissues of *Olfr78*$^{-/-}$ mice than in tumor tissues of WT mice. Moreover, tumor-bearing WT mice developed splenomegaly, a condition in which the spleen is enlarged. However, the spleens of tumor-bearing *Olfr78*$^{-/-}$ mice were similar to those of healthy mice (*SI Appendix*, Fig. S10 *A* and *B*). The populations of total macrophages (*SI Appendix*, Fig. S10*C*), M2-TAMs (*SI Appendix*, Fig. S10*D*), M1 macrophages (*SI Appendix*, Fig. S10*E*), MDSCs (*SI Appendix*, Fig. S10*F*), and Tregs (*SI Appendix*, Fig. S10*G*) were smaller, while those of CD8+ T cells (*SI Appendix*, Fig. S10*H*), but not of CD4+ T cells (*SI Appendix*, Fig. S10*I*), were larger, in spleens of *Olfr78*$^{-/-}$ mice than in spleens of WT mice. Similar to LLC tumors, upon implantation of EO771 syngeneic mouse breast tumor cells into mammary fat pads, tumor growth was significantly ($P < 0.001$) slower (*SI Appendix*, Fig. S11*A*), the survival rate was significantly ($P < 0.001$) better (*SI Appendix*, Fig. S11*B*), and the number of metastatic nodules in the lung was significantly ($P < 0.001$) lower (*SI Appendix*, Fig. S11*C*) in *Olfr78*$^{-/-}$ mice than in WT mice. OR51E2 is highly expressed in prostate cancer patients, prostate cancer cells, and several normal cell types (6, 31, 32). To exclude the possibility that lactate affected tumor growth through Olfr78 on tumor cells, we measured expression of Olfr78 in EO771 tumors. Olfr78 expression was negligible (*SI Appendix*, Fig. S11*D*). These results suggest that macrophage Olfr78 plays a crucial role in maintenance of an immunosuppressive TME and is thereby a key player in tumor progression and metastasis in vivo.

To further examine the involvement of macrophages in tumor progression, we depleted these cells using clodronate liposomes in LLC tumor–bearing mice (33). Depletion of macrophages in tumor-bearing mice decreased the tumor volume (*SI Appendix*, Fig. S12*A*), tumor weight (*SI Appendix*, Fig. S12*B*), and population of total macrophages in the tumor (*SI Appendix*, Fig. S12*C*) and spleen (*SI Appendix*, Fig. S12*D*) such that they were comparable to those in *Olfr78*$^{-/-}$ mice.

To determine the clinical significance of OR51E2 in several cancers such as invasive breast carcinoma, glioblastoma, and lung adenocarcinoma, we searched The Cancer Genome Atlas (TCGA) for treatment analysis reports, gene expression data, and survival results. Based on patient survival data in TCGA, lower OR51E2 expression significantly correlated with longer Kaplan–Meier survival (*SI Appendix*, Fig. S13 *A–C*). The mRNA expression level of OR51E2 significantly ($P < 0.001$) differed between the two patient groups for the three cancers (*SI Appendix*, Fig. S13 *D–F*). However, changes in patients' survival were not dependent on Gpr132 expression (*SI Appendix*, Fig. S13 *G–I*). Taken together,

Vadevoo et al.
The macrophage odorant receptor Olfr78 mediates the lactate-induced M2 phenotype of tumor-associated macrophages

PNAS | 5 of 11
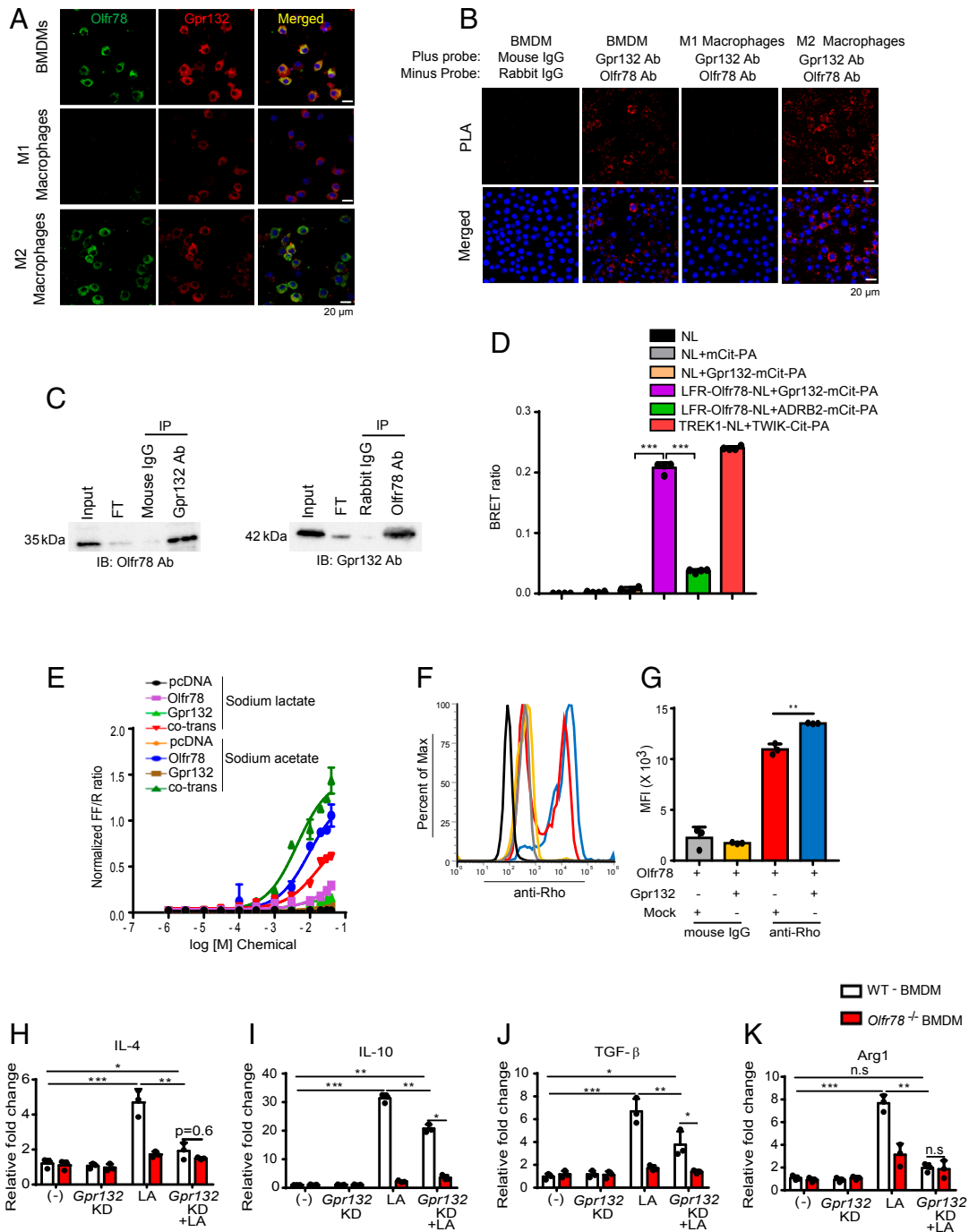https://doi.org/10.1073/pnas.2102434118

Fig. 3. Olfr78 forms a heterodimer with Gpr132 to mediate lactate-induced M2 polarization of mouse BMDMs. (*A*) Confocal microscopic analysis of Olfr78 (green) and Gpr132 (red) expression and their colocalization in BMDMs isolated from mice after treatment with L+I to induce M1 polarization and IL-4 to induce M2 polarization. (Scale bars, 20 μm.) (*B*) A PLA to detect Olfr78 and Gpr132 heterodimerization on the surface of BMDMs and M1 and M2 macrophages. (Scale bars, 20 μm.) (*A* and *B*) Images are representative of three independent experiments. (*C*) Coimmunoprecipitation (IP) and immunoblotting (IB) of Olfr78 and Gpr132 using a rabbit anti-Olfr78 antibody or rabbit normal IgG and a mouse anti-Gpr132 antibody or mouse normal IgG. Input, M2-BMDM cell lysate. FT, flowthrough. Data are representative of three independent experiments. (*D*) BRET ratios for the LFR–Olfr78–Gpr132 and TREK1–TWIK1 interactions. Data represent mean ± SD of *n* = 4 from a representative of three independent experiments. ***P < 0.001. Statistical analysis was performed using a one-way ANOVA with Tukey's multiple-comparison test. (*E*) Relative luciferase activity of Olfr78, Gpr132, and Olfr78/Gpr132 in response to treatment with different concentrations of sodium lactate and sodium acetate in Hana3A cells transfected with an Olfr78 and/or Gpr132 expression vector. Data represent mean ± SD of *n* = 5 from a representative of two independent experiments. (*F* and *G*) FACS analysis of Rho-Olfr78 expression in Hana3A cells cotransfected with Gpr132 and Rho-tagged Olfr78. The black histogram represents unstained cells used as a control. Data represent mean ± SD of *n* = 3 from a representative of three independent experiments. (*H*–*K*) qRT-PCR analysis of the mRNA levels of *IL-4* (*H*), *IL-10* (*I*), *TGF-β* (*J*), and *Arg1* (*K*) in WT and *Olfr78*^{−/−} BMDMs after lactate treatment with or without Gpr132 gene knockdown (Gpr132 KD). (-) refers to control BMDMs with no additional treatment. Data represent mean ± SD of *n* = 3 from a representative of three independent experiments. *P < 0.05, **P < 0.01, and ***P < 0.001. Statistical analysis was performed using a one-way ANOVA with Tukey's multiple-comparison test (*D* and *G*) or a two-way ANOVA with the Bonferroni multiple-comparison test (*H*–*K*).
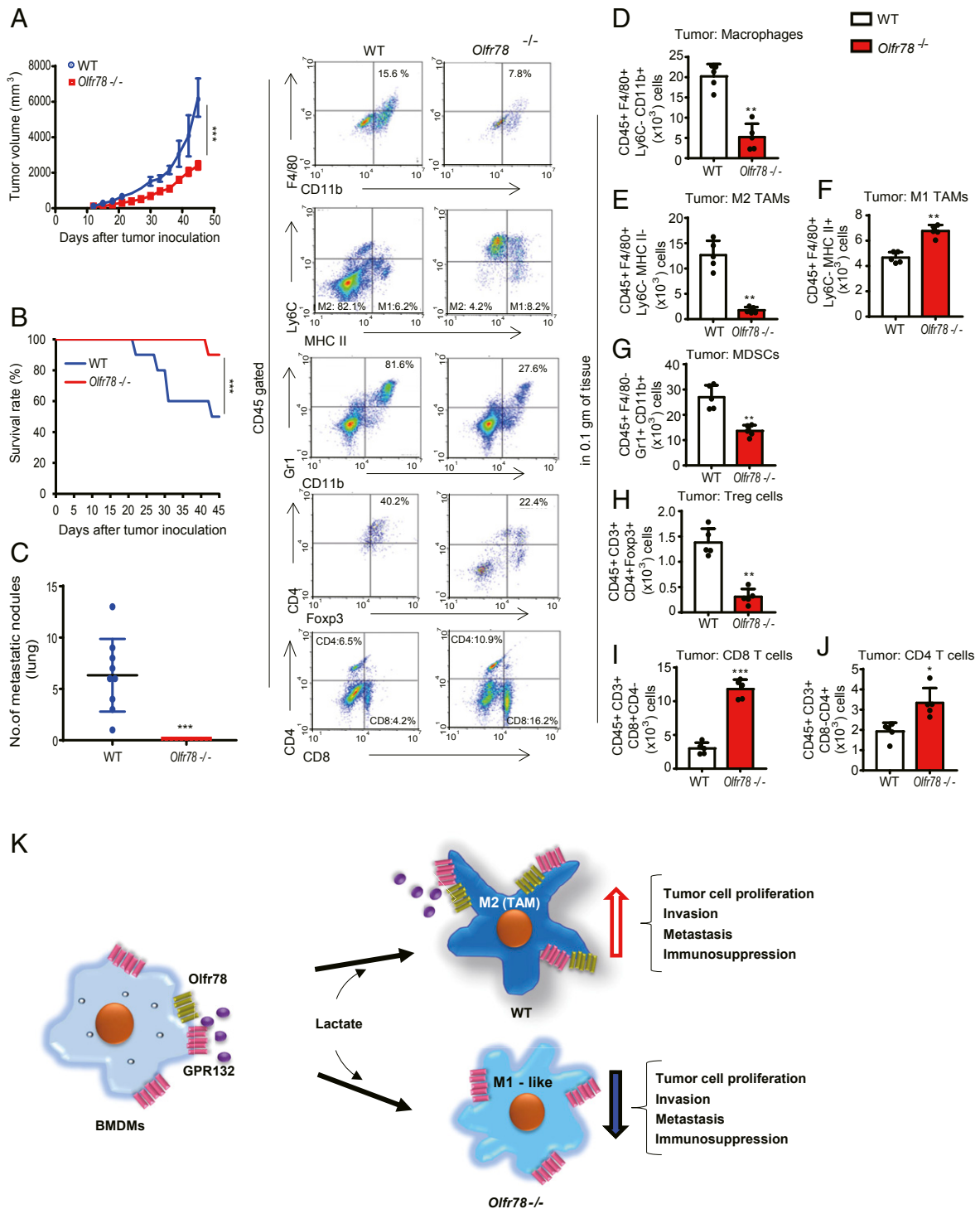
Fig. 4. Depletion of Olfr78 inhibits progression and metastasis of LLC mouse tumors by enhancing antitumor immunity. (*A*) Lung tumor volumes following inoculation of LLC mouse cells into WT and *Olfr78*$^{-/-}$ mice (*n* = 10 mice per group). ***P* < 0.001 by the two-tailed, unpaired *t* test. (*B*) Survival rate of WT and *Olfr78*$^{-/-}$ mice bearing LLC tumors (*n* = 10 mice per group). ***P* < 0.001 by the two-tailed, unpaired *t* test. (*C*) The number of metastatic tumor nodules in the lungs of WT and *Olfr78*$^{-/-}$ mice bearing LLC tumors (*n* = 10 mice per group). ***P* < 0.001 by the two-tailed, unpaired *t* test. (*D–J*) Flow cytometric analysis of CD45+Ly6C–F4/80+CD11b+ total macrophages (*D*), CD45+F4/80+Ly6C–MHCII– M2-polarized TAMs (*E*), CD45+F4/80+Ly6C–MHCII+ M1-polarized TAMs (*F*), CD45+F4/80–Gr1+CD11b+ MDSCs (*G*), CD45+CD3+CD4+Foxp3+ Tregs (*H*), CD45+CD3+CD4–CD8+ T cells (*I*), and CD45+CD3+CD4+CD8– T cells (*J*) among cells isolated from 0.1 g of tumor tissues of WT and *Olfr78*$^{-/-}$ mice. Data represent mean ± SD of *n* = 5 from a representative of three independent experiments. **P* < 0.05, ***P* < 0.01, and ***P* < 0.001 by the two-tailed, unpaired *t* test. (*K*) Schematic diagram of the role of Olfr78 in tumor progression. Macrophages differentiate into TAMs with an M2 phenotype in response to lactate generated in the TME, which promotes tumor progression, invasion, metastasis, and immunosuppression. Lactate induces differentiation of WT BMDMs into protumoral M2-TAMs via the macrophage lactate sensor Olfr78, which functions by forming a heterodimer with Gpr132. However, *Olfr78*$^{-/-}$ BMDMs do not polarize into M2 macrophages in the presence of lactate and therefore do not significantly promote tumor progression and metastasis in syngeneic tumor models, as demonstrated using *Olfr78*$^{-/-}$ mice.

Vadevoo et al.
The macrophage odorant receptor Olfr78 mediates the lactate-induced M2 phenotype of tumor-associated macrophages

PNAS | 7 of 11
https://doi.org/10.1073/pnas.2102434118

these results suggest that perturbation of the Olfr78–lactate interaction may block metastasis in vivo and improve survival by impairing M2 macrophage activation.

Discussion

In this study, we demonstrated that Olfr78, which is primarily expressed in BMDMs, recognizes lactate and acetate derived from tumors, mediates lactate-induced M2 polarization of macrophages, and promotes tumor progression and metastasis in mice. Similar to mouse BMDMs, the interaction of lactate with OR51E2, a human protein analogous to mouse Olfr78, induces M2 polarization of THP-1 human macrophages. Moreover, Olfr78 forms a heterodimer with Gpr132 to promote M2 macrophage polarization. These findings suggest that macrophage Olfr78, together with Gpr132, mediates lactate-induced M2 polarization to generate TAMs in the TME and subsequently promotes tumor progression and metastasis. It is important to elucidate the molecular basis of this interaction because lactate secreted by tumors induces differentiation of macrophages into TAMs that promote tumor progression and metastasis (Fig. 4K). Moreover, identification of the Olfr78–lactate interaction as a therapeutic target may provide fundamental insights into the control of tumor growth and metastasis.

Recently, studies of the expression and function of ectopic ORs in many nonolfactory tissues and cells have increased rapidly (4, 9). Many ectopic ORs are expressed in peripheral immune cells such as monocytes, polymorphonuclear leukocytes (34), and pulmonary macrophages (35). Expression of eight ORs in lung macrophages is synergistically up-regulated by LPS and IFN-γ, leading to M1 polarization. These ORs are suggested to regulate macrophage function by controlling MCP-1 production and cell migration (35). We previously reported the expression and interaction of an ectopic OR with its ligand in brain immune cells, including astrocytes (36, 37) and microglia (38). Microglial ORs recognize pathogen-derived metabolites and induce activation of microglia to perform chemotaxis, cytokine production, phagocytosis, and reactive oxygen species generation (38). In this study, we showed that Olfr78 was expressed in M2, but not M1, macrophages, suggesting it is an M2-specific marker. Moreover, we demonstrated that Olfr78 mediated lactate-induced generation of protumoral M2-TAMs using isolated Olfr78$^{-/-}$ BMDMs with or without exogenous Olfr78 expression. In addition to the immune system, many ORs are expressed in tumor cells (4, 9, 11). Such ORs are not only biomarkers of tumor cells but also appear to affect tumor cell proliferation and tumor progression (4, 9, 11, 39). OR51E2, also named prostate-specific GPCR, is specifically up-regulated in prostate cancer, suggesting it as an immunotherapeutic target (40–42). Activation of OR51E2 by β-ionone, a steroid derivative, inhibits cancer cell proliferation (43, 44). The function of OR51E2 in tumor cells is currently being debated. Under our experimental conditions, Olfr78$^{-/-}$ BMDMs and OR51E2-depleted human macrophages did not undergo M2 polarization in response to lactate. Reexpression of Olfr78 restored lactate-mediated M2 polarization of Olfr78$^{-/-}$ BMDMs. Moreover, tumor growth and metastasis were inhibited in syngeneic Olfr78-deficient mice compared with WT mice. To study the in vivo role of target genes in tumors, a human tumor cell line–derived xenograft in immunodeficient mice is the gold standard. However, the immune system is a key component of the TME and very important for the host's defense against tumor progression (45). Therefore, it is more desirable to study an immunocompetent mouse model with syngeneic tumor cells implanted at an orthotropic location. The LLC tumor and EO771 breast tumor models used in this study are syngeneic, rather than xenograft, mouse tumor models, and are useful for studying tumor–immune cell interactions (46, 47). An EO771 breast tumor was orthotropically implanted into the mouse mammary gland to further mimic the TME. Taken together, these data suggest that macrophage

Olfr78 mediates lactate-induced M2 polarization of TAMs in the TME and subsequently promotes tumor progression and metastasis. Nevertheless, because tumor progression and metastasis were analyzed in Olfr78$^{-/-}$ mice, the possibility that Olfr78 expression in cells other than macrophages contributes to the observed effects cannot be completely excluded. To overcome this limitation, a conditional knockout mouse should be generated in a future study.

Olfr78 and Gpr132 form a heterodimer to mediate M2 polarization of macrophages. In this study, confocal microscopy and a PLA demonstrated that Olfr78 and Gpr132 colocalized on the membrane of BMDMs and M2 macrophages. In addition, Olfr78 was coimmunoprecipitated by an anti-Gpr132 antibody and vice versa. Furthermore, independent BRET analysis showed a close interaction between Olfr78 and Gpr132. Functionally, we showed that lactate synergistically affected Olfr78 and Gpr132, and Gpr132 enhanced surface expression of Olfr78. Deficiency of Olfr78 or Gpr132 reduced lactate-mediated M2 polarization of BMDMs, and this effect was enhanced by deficiency of both proteins. These findings suggest that Olfr78 and Gpr132 form a heterodimer in the membrane of BMDMs and M2 macrophages and cooperate to promote M2 macrophage polarization. Consistently, GPCRs have been reported to form dimers as part of their normal trafficking and function (12). Certain GPCRs have a strict requirement for heterodimerization to attain proper surface expression and functional activity (12). For example, heterodimerization of the olfactory receptor M71 with the GPCR ADRB2 enhances not only surface expression of M71 but also the functional activity of M71 and cointernalization of M71 and ADRB2 upon stimulation (15). We suggest that heterodimerization of Olfr78 and Gpr132 enhances surface expression of Olfr78 and their functional activity in response to lactate.

IL-4–induced M2 polarization of macrophages was not inhibited by Olfr78 deficiency or Gpr132 deficiency (22). These findings suggest that IL-4 induces M2 polarization of macrophages through a different pathway from that dependent on Olfr78 and Gpr132. On the other hand, knockout of Gpr137b reduces IL-4–induced M2 polarization of macrophages (48). In addition, inhibition of CSF-1R blocks M2 polarization of macrophages (49). Collectively, these findings suggest that multiple receptors, including Olfr78, Gpr132, Gpr137b, and CSF-1R, are involved in M2 polarization of TAMs in the TME.

In summary, results reported here provide evidence that the OR Olfr78 forms a heterodimer with Gpr132 that senses lactate in the TME and mediates lactate-induced generation of protumoral M2-TAMs to promote tumor progression. Taken together, the findings of this study suggest that Olfr78 may be a target for cancer therapy. Further studies of Olfr78 need to investigate dynamic networks among tumor cells, M2-polarized TAMs, and other infiltrating immune cells in the TME.

Materials and Methods

Cell Culture. LLC and B16F10 melanoma mouse tumor cell lines and the MDA MB231 human breast tumor cell line were cultured in Dulbecco's modified Eagle's medium (DMEM; HyClone). The 4T1 mouse breast tumor cell line and the MCF7 breast and A549 lung human tumor cell lines were cultured in RPMI medium (HyClone). All cell cultures were supplemented with 10% fetal bovine serum (FBS; Thermo Fisher Scientific) and maintained at 37 °C in a humidified atmosphere containing 5% CO_2.

M1 and M2 Polarization of BMDMs. BMDMs were isolated from tibias and femurs of C57BL6 mice and cultured in DMEM supplemented with 10 ng/mL macrophage colony-stimulating factor (Gibco) and 10% FBS for 7 d. The culture medium was changed every other day. For M1 polarization, BMDMs were incubated with 20 ng/mL recombinant mouse IFN-γ (R&D Systems) plus 100 ng/mL LPS for 24 to 48 h. For M2 polarization, BMDMs were incubated with 20 ng/mL recombinant mouse IL-4 for 24 to 48 h. For lactate-mediated M2 polarization, BMDMs were treated with 10 mM lactate (Sigma-Aldrich) at 37 °C in a humidified atmosphere containing 5% CO_2 for 24 to 48 h.

Flow Cytometry. Anti-CD11b, anti-CD3, anti-CD4, anti-CD8, anti-CD86, anti–F4/80, anti-CD206, anti-CD163, and anti-Gr1 antibodies were purchased from BioLegend. An anti-Olfr78 antibody was purchased from LSBio. Cells were fixed with 4% paraformaldehyde and then incubated with an untagged primary antibody or a dye-tagged antibody at 4 °C for 30 min in the dark. Cells treated with an untagged primary antibody (anti-Olfr78, anti-CD206, and anti-CD86) were washed and incubated with a dye-tagged secondary antibody. At least 10,000 events were analyzed using a flow cytometer (BD Biosciences). Data were evaluated using CellQuest Pro software (BD Biosciences). To prepare cell suspensions from tumor tissues, freshly excised tumors were fragmented into several pieces and minced into 2- to 3-mm^3 pieces, and 0.1 g of tumor tissue was incubated with collagenase D (Roche) and DNase (Sigma-Aldrich) at 37 °C for 40 min. The tissue samples were filtered through a 100-μm cell strainer (Falcon) to collect digested cells. Collected cells were resuspended in phosphate-buffered saline containing FBS and subjected to flow cytometry. The immune cell–gating strategy is described in *SI Appendix*, Fig. S9. Antibody details are listed in *SI Appendix*, Table S1.

qRT-PCR. Cells were lysed using QIAzol lysis reagent (Qiagen). RNA was isolated from cell lysates using an miRNeasy Mini Kit (Qiagen) and subjected to qRT-PCR. Primers targeting *Arg1*, *IL-10*, *IL-4*, *TGF-β*, *IL-12p40*, *IFN-γ*, and *β-actin* were obtained from Bioneer. Complementary DNA (cDNA) was synthesized using a PrimeScript First-Strand cDNA Synthesis Kit (Takara). qPCR using SYBR Green (Qiagen) was performed on a real-time cycler (Bio-Rad). β-Actin was used as an endogenous control. Data used to determine relative expression were analyzed according to the Livak and Schmittgen method (50). The primer sequences were designed (51) and are listed in *SI Appendix*, Table S2.

Immunofluorescence Microscopy. Cells (1×10^5 cells per well in a 4-well chamber) were fixed with 4% paraformaldehyde and incubated with antibodies against Olfr78 and Gpr132 (1:100 dilution; Santa Cruz Biotechnology) at 24 °C for 1 h or at 4 °C for 16 h. Cells were then incubated with fluorophore-tagged secondary antibodies at 24 °C for 1 h. Cells were stained with 4′,6-diamidino-2-phenylindole (DAPI) to label nuclei, mounted with ProLong Gold antifade mounting reagent (Life Technologies), and observed under a confocal microscope. Antibody details are listed in *SI Appendix*, Table S1.

Measurement of Lactate and Acetate Concentrations and Determination of Cytokine Concentrations Using Enzyme-Linked Immunosorbent Assays. The concentrations of lactate and acetate in TCM of cells cultured at 80% confluency were measured using lactate and acetate colorimetric assay kits (BioVision). Briefly, 50 μL of TCM was mixed with lactate or acetate enzyme mix and the probe according to the manual and incubated for 30 min at room temperature. The concentrations of cytokines in the conditioned medium of macrophages were measured using cytokine enzyme-linked immunosorbent assay (ELISA) kits (R&D Systems). Briefly, 100 μL of conditioned medium was added to plates precoated with antibodies against IL-4, IL-10, and TGF-β. Samples were incubated with corresponding antibodies conjugated to biotin and then with horseradish peroxidase–labeled streptavidin. Absorbance at 570 nm was measured using a microplate reader. The concentrations of lactate, acetate, and cytokines were calculated from the standard curves.

PLA. BMDMs were incubated with a rabbit anti-Olfr78 antibody (LifeSpan Biosciences) and a mouse anti-Gpr132 antibody (Santa Cruz Biotechnology) at 24 °C for 1 h. Rabbit immunoglobulin G (IgG) and mouse IgG were used as controls. Cells were then incubated with an anti-rabbit MINUS PLA probe and an anti-mouse PLUS PLA probe at 37 °C for 60 min. After washing, cells were incubated with ligation stocks and ligase mixtures at 37 °C for 30 min and then with amplification stocks and polymerase mixtures at 37 °C for 100 min. Samples were mounted with Duolink In Situ Mounting Medium (Sigma-Aldrich) and observed under a confocal microscope (Nanoscope).

Coimmunoprecipitation Assays and Western Blot Analysis. For coimmunoprecipitation assays, cells were lysed with M-PER Mammalian Protein Extraction Reagent (Thermo Fisher Scientific). Cell lysates were incubated with 2 μg of an antibody against Olfr78 (or rabbit normal IgG) or Gpr132 (or mouse normal IgG) at 4 °C overnight and then with protein A–agarose beads (Thermo Fisher Scientific) at 4 °C for 4 h with agitation. The beads were boiled, and the eluates were subjected to Western blotting with an antibody against Olfr78 or Gpr132. To assess protein expression, 40 μg of protein was electrophoresed on a 10% sodium dodecyl sulfate–polyacrylamide gel and

transferred to a membrane (Millipore). The membrane was incubated with antibodies against iNOS (Abcam), Arg1 (Abcam), and β-actin (Santa Cruz Biotechnology) at 4 °C overnight followed by a horseradish peroxidase–tagged secondary antibody at room temperature for 2 h, and then exposed to a chemiluminescence substrate (Thermo Fisher Scientific). Signals were visualized using an LAS1000 enhanced chemiluminescence detection system (Fujifilm).

Luciferase Assay. Luciferase assays were performed according to a previous report (38) using the Dual-Glo Luciferase Assay System (Promega). Briefly, mock, Olfr78, Gpr132, OR51E2, OR51E2/Gpr132, or Olfr78/Gpr132 transiently transfected Hana3A cells were stimulated with various concentrations of sodium lactate or sodium acetate diluted in CD293 medium at 37 °C for 4 h. The activity of firefly luciferase was normalized against that of *Renilla* luciferase. Luminescence was measured on a SpectraMax L microplate reader (Molecular Devices).

Rho-Olfr78 Surface Expression Study. Surface expression of Olfr78 on Hana3A cells transfected with Rho-tagged Olfr78 with or without Gpr132 was determined by fluorescence-activated cell sorting (FACS) analysis of Rho expression using an anti-Rho antibody. Briefly, mock, Olfr78, Gpr132, or Olfr78/Gpr132 transiently transfected Hana3A cells were fixed with 4% paraformaldehyde and then incubated with an untagged primary antibody (anti-Rho) or IgG control (mouse IgG) at 4 °C for 30 min, washed, and incubated with a dye-tagged secondary antibody. At least 10,000 events were analyzed using a flow cytometer (Attune NxT; Invitrogen). Data were evaluated using Attune NxT software (Invitrogen).

Construction of BRET Plasmids. The lucy-flag-rho (LFR)-Olfr78-pME18s and Gpr132-HA-pcDNA3.1 expression vectors were used as templates for a PCR-based Gateway cloning method (Invitrogen). The primers used for PCR were as follows: forward primer for LFR-Olfr78 with an *att* site, 5′-GGGGACAAG-TTTGTACAAAAAAGCAGGCTCCACCATGAGACCCCAGATCCTGCT-3′; and reverse primer for LFR-Olfr78 with an *att* site, 5′-GGGGACCACTTTGTACAAGAA-AGCTGGGTTCGTGTTTCCCCCAGCTTCAA-3′; forward primer for Gpr132 with an *att* site, 5′-GGGGACAAGTTTGTACAAAAAAGCAGGCTCCACCATGAGATCAGA-ACCTACCAA-3′; and reverse primer for Gpr132 with an *att* site, 5′-GGGGAC-CACTTTGTACAAGAAAGCTGGGTTGCAGAGCTCCTCAGGCAGTC-3′. Each PCR fragment was cloned into the pDONR207 vector via the BP recombination reaction of the Gateway cloning system (Invitrogen). cDNAs encoding full-length mouse TREK1 (GenBank accession no. NM_010607), mouse TWIK1 (NM_008430), and human ADRB2 (NM_000024) were cloned into the pDONR207 vector using an RT-PCR–based Gateway cloning method (Invitrogen). These pDONR207 entry vectors were sequenced and the sequences of the cloned cDNAs were confirmed. Next, the LR reaction of the Gateway cloning system was performed with these entry vectors and destination vectors for the BRET assay (pLenti GW-mCit-PA, Addgene plasmid 113457; pLenti GW-NL-myc, Addgene plasmid 113455) (29). Finally, the expression vectors LFR-Olfr78-NL, LFR-Olfr78-mCit-PA, Gpr132-mCit-PA, ADRB2-mCit-PA, TREK1-NL, and TWIK1-mCit-PA were constructed for the BRET assay.

BRET Assay. Hana3A cells were cultured in 35-mm culture dishes (SPL) at a density of 5.0 to 5.5×10^5 cells per dish at 37 °C in an atmosphere containing 5% CO_2 in 2 mL of complete medium (DMEM/high glucose containing 100 IU/mL penicillin) supplemented with 10% FBS (Gibco). After 24 h, cells were transfected with plasmids encoding donor and acceptor proteins at a ratio of 1:10 (total 3 μg of DNA) using Lipofectamine 2000. Transfected cells were detached after 24 h with TrypLE (Gibco), resuspended in complete medium, and plated in 96-well cell-culture plates (SPL) at a density of 4.0 to 4.5×10^4 cells per well. Cells were maintained at 37 °C in an atmosphere containing 5% CO_2 for a further 24 h to allow them to adhere before performing the BRET assay. Cells were treated with coelenterazine-h (Sigma-Aldrich) at a final concentration of 5 μM (total volume of 50 μL per well) and incubated for an additional 15 min. An M1000Pro microplate reader (TECAN) was used with an integration time of 1 s to measure the short and long wavelengths with BLUE1 (370 to 480 nm) and GREEN1 (520 to 570 nm) filters. BRET ratios were calculated as (long-wavelength emission/short-wavelength emission) − (long-wavelength emission for donor NanoLuc Luciferase [NL]-only transfected cells/short-wavelength emission for donor [NL]-only transfected cells).

Transfection and Expression of Olfr78. The LFR-Olfr78-pME18s expression vector was constructed and transfected into *Olfr78*$^{-/-}$ BMDMs. For transfection, cells (1×10^5) were incubated in 100 μL of antibiotic-free Opti-MEM

Vadevoo et al.
The macrophage odorant receptor Olfr78 mediates the lactate-induced M2 phenotype of
tumor-associated macrophages

PNAS | 9 of 11
https://doi.org/10.1073/pnas.2102434118

medium and transfected with 0.5 μg of the Olfr78 expression vector using 2 μL of Lipofectamine 2000 (Thermo Fisher Scientific). Expression of Olfr78 was confirmed by immunofluorescence staining using antibodies against Flag and Olfr78. An anti-Flag antibody was purchased from Sigma-Aldrich and an anti-Olfr78 antibody was purchased from LSBio. Details of the antibodies used for the various analyses are provided in *SI Appendix*, Table S1.

siRNA Transfection. siRNAs against OR51E2 and mouse Gpr132 were purchased from Bioneer and Dharmacon, respectively. Control siRNA was purchased from Bioneer (*SI Appendix*, Table S3). BMDMs (1×10^5) were incubated in 100 μL of antibiotic-free Opti-MEM medium and transfected with 50 nM siRNA using 2 μL of Lipofectamine RNAiMAX (Thermo Fisher Scientific). Gene knockdown was confirmed by Western blot analysis. The siRNA sequences are listed in *SI Appendix*, Table S3.

Animal Models. C57BL6 mice aged 6 to 8 wk were purchased from Orient Bio. $Olfr78^{-/-}$ C57BL6 mice were kindly provided by Jennifer Pluznick, Johns Hopkins University, Baltimore, MD. Mice were cared for and maintained in accordance with the guidelines of the Institutional Animal Care and Use Committee of Kyungpook National University (Permission no. 2015-0017) or the Daegu Gyeongbuk Institute of Science and Technology. The LLC syngeneic lung tumor model was prepared by subcutaneously injecting 1×10^6 LLC cells into the lower right flank of male mice. The EO771 syngeneic breast tumor model was prepared by implanting 1×10^6 EO771 cells into the lower left mammary fat pad of female mice. At the end of treatment, mice were killed for analysis of immune cells in tumors and the spleen or maintained to determine the survival rate.

Statistical Analysis. All data are expressed as mean ± SD unless otherwise noted. All statistical analyses were performed using Prism software (GraphPad Software). Statistical significance was determined by a one-way ANOVA with Tukey's multiple-comparison test, a two-way ANOVA with the Bonferroni multiple-comparison test, and the Student's *t* test. $P < 0.05$ was considered significant.

Data Availability. All study data are included in the article and/or *SI Appendix*.

1. W. K. Kroeze, D. J. Sheffler, B. L. Roth, G-protein-coupled receptors at a glance. *J. Cell Sci.* **116**, 4867–4869 (2003).
2. T. K. Bjarnadóttir et al., Comprehensive repertoire and phylogenetic analysis of the G protein-coupled receptors in human and mouse. *Genomics* **88**, 263–273 (2006).
3. A. S. Hauser, M. M. Attwood, M. Rask-Andersen, H. B. Schiöth, D. E. Gloriam, Trends in GPCR drug discovery: New agents, targets and indications. *Nat. Rev. Drug Discov.* **16**, 829–842 (2017).
4. N. Kang, J. Koo, Olfactory receptors in non-chemosensory tissues. *BMB Rep.* **45**, 612–622 (2012).
5. N. Kang et al., Olfactory marker protein expression is an indicator of olfactory receptor-associated events in non-olfactory tissues. *PLoS One* **10**, e0116097 (2015).
6. C. Flegel, S. Manteniotis, S. Osthold, H. Hatt, G. Gisselmann, Expression profile of ectopic olfactory receptors determined by deep sequencing. *PLoS One* **8**, e55368 (2013).
7. *Tabula Muris* Consortium et al., Single-cell transcriptomics of 20 mouse organs creates a *Tabula Muris*. *Nature* **562**, 367–372 (2018).
8. S. Kalra et al., Analysis of single-cell transcriptomes links enrichment of olfactory receptors with cancer cell differentiation status and prognosis. *Commun. Biol.* **3**, 506 (2020).
9. D. Maßberg, H. Hatt, Human olfactory receptors: Novel cellular functions outside of the nose. *Physiol. Rev.* **98**, 1739–1763 (2018).
10. S.-J. Lee, I. Depoortere, H. Hatt, Therapeutic potential of ectopic olfactory and taste receptors. *Nat. Rev. Drug Discov.* **18**, 116–138 (2019).
11. A. Di Pizio, M. Behrens, D. Krautwurst, Beyond the flavour: The potential druggability of chemosensory G protein-coupled receptors. *Int. J. Mol. Sci.* **20**, 1402 (2019).
12. S. C. Prinster, C. Hague, R. A. Hall, Heterodimerization of G protein-coupled receptors: Specificity and functional significance. *Pharmacol. Rev.* **57**, 289–298 (2005).
13. Y.-H. Huang, Y.-S. Su, C.-J. Chang, W.-H. Sun, Heteromerization of G2A and OGR1 enhances proton sensitivity and proton-induced calcium signals. *J. Recept. Signal Transduct. Res.* **36**, 633–644 (2016).
14. P. Lin, R. D. Ye, The lysophospholipid receptor G2A activates a specific combination of G proteins and promotes apoptosis. *J. Biol. Chem.* **278**, 14379–14386 (2003).
15. C. Hague et al., Olfactory receptor surface expression is driven by association with the β₂-adrenergic receptor. *Proc. Natl. Acad. Sci. U.S.A.* **101**, 13672–13676 (2004).
16. G. Solinas, G. Germano, A. Mantovani, P. Allavena, Tumor-associated macrophages (TAM) as major players of the cancer-related inflammation. *J. Leukoc. Biol.* **86**, 1065–1073 (2009).
17. T. Chanmee, P. Ontong, K. Konno, N. Itano, Tumor-associated macrophages as major players in the tumor microenvironment. *Cancers (Basel)* **6**, 1670–1690 (2014).
18. A. Sica, T. Schioppa, A. Mantovani, P. Allavena, Tumour-associated macrophages are a distinct M2 polarised population promoting tumour progression: Potential targets of anti-cancer therapy. *Eur. J. Cancer* **42**, 717–727 (2006).
19. O. R. Colegio et al., Functional polarization of tumour-associated macrophages by tumour-derived lactic acid. *Nature* **513**, 559–563 (2014).
20. A. Mantovani et al., The chemokine system in diverse forms of macrophage activation and polarization. *Trends Immunol.* **25**, 677–686 (2004).
21. L. Ippolito, A. Morandi, E. Giannoni, P. Chiarugi, Lactate: A metabolic driver in the tumour landscape. *Trends Biochem. Sci.* **44**, 153–166 (2019).
22. P. Chen et al., Gpr132 sensing of lactate mediates tumor-macrophage interplay to promote breast cancer metastasis. *Proc. Natl. Acad. Sci. U.S.A.* **114**, 580–585 (2017).
23. A. J. Chang, F. E. Ortega, J. Riegler, D. V. Madison, M. A. Krasnow, Oxygen regulation of breathing through an olfactory receptor activated by lactate. *Nature* **527**, 240–244 (2015).
24. W. H. Aisenberg et al., Defining an olfactory receptor function in airway smooth muscle cells. *Sci. Rep.* **6**, 38231 (2016).
25. M. Stein, S. Keshav, N. Harris, S. Gordon, Interleukin 4 potently enhances murine macrophage mannose receptor activity: A marker of alternative immunologic macrophage activation. *J. Exp. Med.* **176**, 287–292 (1992).
26. S. Gordon, F. O. Martinez, Alternative activation of macrophages: Mechanism and functions. *Immunity* **32**, 593–604 (2010).
27. S. Su et al., A positive feedback loop between mesenchymal-like cancer cells and macrophages is essential to breast cancer metastasis. *Cancer Cell* **25**, 605–620 (2014).
28. J. L. Pluznick et al., Olfactory receptor responding to gut microbiota-derived signals plays a role in renin secretion and blood pressure regulation. *Proc. Natl. Acad. Sci. U.S.A.* **110**, 4410–4415 (2013).
29. P. Trepte et al., LuTHy: A double-readout bioluminescence-based two-hybrid technology for quantitative mapping of protein-protein interactions in mammalian cells. *Mol. Syst. Biol.* **14**, e8071 (2018).
30. E. M. Hwang et al., A disulphide-linked heterodimer of TWIK-1 and TREK-1 mediates passive conductance in astrocytes. *Nat. Commun.* **5**, 3227 (2014).
31. M. F. Souza et al., Circulating mRNAs and miRNAs as candidate markers for the diagnosis and prognosis of prostate cancer. *PLoS One* **12**, e0184094 (2017).
32. D. Maßberg et al., The activation of OR51E1 causes growth suppression of human prostate cancer cells. *Oncotarget* **7**, 48231–48249 (2016).
33. S. M. Zeisberger et al., Clodronate-liposome-mediated depletion of tumour-associated macrophages: A new and highly effective antiangiogenic therapy approach. *Br. J. Cancer* **95**, 272–281 (2006).
34. A. Malki et al., Class I odorant receptors, TAS1R and TAS2R taste receptors, are markers for subpopulations of circulating leukocytes. *J. Leukoc. Biol.* **97**, 533–545 (2015).
35. J. J. Li et al., Activation of olfactory receptors on mouse pulmonary macrophages promotes monocyte chemotactic protein-1 production. *PLoS One* **8**, e80148 (2013).
36. T. Cho, C. Lee, N. Lee, Y. R. Hong, J. Koo, Small-chain fatty acid activates astrocytic odorant receptor Olfr920. *Biochem. Biophys. Res. Commun.* **510**, 383–387 (2019).
37. N. Lee, M. Sa, Y. R. Hong, C. J. Lee, J. Koo, Fatty acid increases cAMP-dependent lactate and MAO-B-dependent GABA production in mouse astrocytes by activating a $G_{\alpha s}$ protein-coupled receptor. *Exp. Neurobiol.* **27**, 365–376 (2018).
38. N. Lee et al., A pathogen-derived metabolite induces microglial activation via odorant receptors. *FEBS J.* **287**, 3841–3870 (2020).
39. N. M. Dalesio, S. F. Barreto Ortiz, J. L. Pluznick, D. E. Berkowitz, Olfactory, taste, and photo sensory receptors in non-sensory organs: It just makes sense. *Front. Physiol.* **9**, 1673 (2018).
40. L. L. Xu et al., PSGR, a novel prostate-specific gene with homology to a G protein-coupled receptor, is overexpressed in prostate cancer. *Cancer Res.* **60**, 6568–6572 (2000).
41. M. Rodriguez et al., PSGR promotes prostatic intraepithelial neoplasia and prostate cancer xenograft growth through NF-κB. *Oncogenesis* **3**, e114 (2014).

42. M. Rodriguez *et al.*, Prostate-specific G-protein-coupled receptor collaborates with loss of PTEN to promote prostate cancer progression. *Oncogene* **35**, 1153–1162 (2016).

43. E. M. Neuhaus *et al.*, Activation of an olfactory receptor inhibits proliferation of prostate cancer cells. *J. Biol. Chem.* **284**, 16218–16225 (2009).

44. N. Jovancevic *et al.*, Odorant receptor 51E2 agonist β-ionone regulates RPE cell migration and proliferation. *Front. Physiol.* **8**, 888 (2017).

45. R. Rosenthal *et al.*; TRACERx Consortium, Neoantigen-directed immune escape in lung cancer evolution. *Nature* **567**, 479–485 (2019).

46. M. P. Keane, J. A. Belperio, Y. Y. Xue, M. D. Burdick, R. M. Strieter, Depletion of CXCR2 inhibits tumor growth and angiogenesis in a murine model of lung cancer. *J. Immunol.* **172**, 2853–2860 (2004).

47. A. S. Betof *et al.*, Modulation of murine breast tumor vascularity, hypoxia and chemotherapeutic response by exercise. *J. Natl. Cancer Inst.* **107**, djv040 (2015).

48. Z. Islam, T. Inui, O. Ishibashi, Gpr137b is an orphan G-protein-coupled receptor associated with M2 macrophage polarization. *Biochem. Biophys. Res. Commun.* **509**, 657–663 (2019).

49. S. M. Pyonteck *et al.*, CSF-1R inhibition alters macrophage polarization and blocks glioma progression. *Nat. Med.* **19**, 1264–1272 (2013).

50. K. J. Livak, T. D. Schmittgen, Analysis of relative gene expression data using real-time quantitative PCR and the 2(−ΔΔC(T)) method. *Methods* **25**, 402–408 (2001).

51. H. Kim, N. Kang, K. An, J. Koo, M.-S. Kim, MRPrimerW: A tool for rapid design of valid high-quality primers for multiple target qPCR experiments. *Nucleic Acids Res.* **44**, W259–W266 (2016).

Vadevoo et al.
The macrophage odorant receptor Olfr78 mediates the lactate-induced M2 phenotype of tumor-associated macrophages

PNAS | **11 of 11**
https://doi.org/10.1073/pnas.2102434118